CrossMark

Possible Detection of a Flare-associated Coronal Mass Ejection on an M-dwarf

J. Wang[1,2]

[1] Guangxi Key Laboratory for Relativistic Astrophysics, School of Physical Science and Technology, Guangxi University, Nanning 530004, China; wj@nao.cas.cn
[2] Key Laboratory of Space Astronomy and Technology, National Astronomical Observatories, Chinese Academy of Sciences, Beijing 100101, China

Abstract

We here report a probable detection of a stellar coronal mass ejection (CME) in active M dwarf KIC 8093473 by performing an analysis on its time resolved X-ray spectra observed by the XMM-Newton satellite. Compared to the value at the quiescent state and the interstellar one, our spectral modeling returns a marginal (and probably evolving) excess of hydrogen column density in the flare state at a significance level of 1σ, which can be understood by an additional absorption due to a flare-associate CME. The CME mass is then estimated to be $\sim 7 \times 10^{18}$–2×10^{20} g according to the ice cream cone model.

Key words: stars: coronae – stars: flare – stars: late-type – X-rays: stars

1. Introduction

As an analogy with the Sun, a stellar coronal mass ejection (CME, e.g., Leitzinger & Odert 2022), manifested by a large scale expulsion of the confined and magnetized plasma into interplanetary space (e.g., Kahler 1992; Tsuneta 1996; Kliem et al. 2000; Karlicky & Barta 2007; Li et al. 2016; Jiang et al. 2021), is expected for solar-like and late-type main-sequence stars. The study of stellar CMEs is essential for evaluating the habitability of an exoplanet, especially for nearby M dwarfs (Shields et al. 2016) that are associated with a habitable zone with a distance less than 0.1 au from the host stars. Theoretically, frequent stellar CMEs can tear off most of the atmosphere of an exoplanet (e.g., Khodachenko et al. 2007; Cherenkov et al. 2017), and compress the magnetosphere, which enables a penetration of energetic particles into the planetary atmosphere. The subsequent atmospheric chemistry simulations indicate an enhanced production of the greenhouse gas nitrous oxide and HCN in the atmosphere (e.g., Tian et al. 2011; Airapetian et al. 2016; Barnes et al. 2016).

However, due to a lack of enough spatial resolution, detection of a stellar CME is still a hard task for current instruments. We refer the readers to Moschou et al. (2019) and Osten & Wolk (2017) for reviews on the methods of detection of stellar CMEs. Generally speaking, a handful of stellar CME candidates have been reported previously according to either high velocity Balmer line wings or blueshifted emission lines in X-ray (e.g., Houdebine et al. 1990; Argiroffi et al. 2019; Koller et al. 2021; Namekata et al. 2021; Wang et al. 2021; Lu et al. 2022; Wang et al. 2022; Wu et al. 2022). Other claims of detection of a stellar CME include an observed extreme ultraviolet (EUV)/X-ray dimming (e.g., Ambruster et al. 1989; Chandra et al. 2016; Veronig et al. 2021) and a pre-flare dip in

an optical light curve (e.g., Giampapa et al. 1982; Leitzinger et al. 2014), although the latter has been argued against since the dip could have also resulted from an increase in H^- opacity during a flare.

Additionally, an increased column density revealed in an X-ray spectrum, due to absorption by an expanding CME, can be used as an indirect CME signature. In fact, Franciosini et al. (2001) reported that the column density N_H during a flare is higher than the quiescent value by a factor of 5 in a large long-duration X-ray flare in the RS CVn binary system UX Arietis. The temporal decay of the X-ray absorption during a superflare on the eclipsing binary Algol measured by Favata & Schmitt (1999) was then explained as a signature of a CME by Moschou et al. (2017).

In this paper, we report a probable flare-associated CME from an M dwarf, KIC 8093473, according to its increased N_H during a flare revealed by our time-resolved X-ray spectral analysis, thanks to the coordinated observations taken by both Kepler and XMM-Newton. The paper is organized as follows. Section 2 presents a description of the target. The time-resolved X-ray spectra are analyzed in Section 3. Section 4 provides the results and discussions.

2. KIC 8093473

Kuznetsov & Kolotkov (2021) recently matched the Kepler (Borucki et al. 2010) and XMM-Newton (Jansen et al. 2001) simultaneous flare observations, which enabled the authors to successfully identify nine flares in three late type stars; they are KIC 8093473, KIC 8454353 and KIC 9048551. After examining the raw XMM-Newton data, we focus here only on KIC 8093473 simply because one of its X-ray flares shows

enough photon counts for subsequent modeling on time resolved X-ray spectra.

KIC 8093473 (=2MASS J19212847+4355456) is a low-mass ($M_\star = 0.274\ M_\odot$) flaring star with an effective temperature of 3357^{+171}_{-87} K and a distance of $205.9^{+8.0}_{-7.5}$ pc taken from the Gaia Data Release 2 catalog (Gaia Collaboration et al. 2018). A total of 438 flares has been detected in the object from the whole long-cadence data (Van Cleve et al. 2016, Data Release 25, Q1–Q17, 48 months) of the Kepler mission by a comprehensive study carried out by Yang & Liu (2019). The released energy of the detected flares ranges from $10^{31.7-33.9}$ erg. Since it is above the main sequence (see Figure 1 in Kuznetsov & Kolotkov 2021), Kuznetsov & Kolotkov (2021) argued that KIC 8093473 with a measured spectral type of M3 (Pecaut & Mamajek 2013) is most likely an unresolved binary or a multiple system consisting of M-dwarfs.

3. Analysis and Results

We attempt to examine the probable CME feature of the object in this section by comparing the flaring and quiescent X-ray spectral properties obtained from our X-ray spectral modeling. With this motivation, we at first need to reproduce the X-ray light curve not only in the flaring state, but also in the quiescent state. In fact, the latter is quite important for extracting a quiescent spectrum with adequate signal-to-noise ratio.

3.1. X-Ray Light Curves

The object has been observed in three runs (i.e., Obs. ID = 0302150101, 0302150201 and 0600040101) from 2005 to 2009 by the XMM-Newton onboard EPIC cameras. However, the observation run of Obs.ID = 0302150201 is discarded in the subsequent analysis simply because the source is heavily contaminated by the bad pixel column.

For each of the two remaining observational runs, the EPIC PN (Struder et al. 2001) data are reduced by the SAS v19.1 software[3] and by the corresponding calibration files. The events corresponding to patterns 0–4 are selected from the PN data and the CCD chip gaps are avoided. The bad and hot pixels are then removed from the original images. The light curve of the source is then extracted from a circular aperture at the source position with a radius of 15″. The background light curve is obtained from a circular source-free region with a radius of 45″, which is offset from, but close to, the source. The SAS tasks *epatplot* and *epiclccorr* are used for pile-up effect checking and to produce background removed light curves, respectively.

---

[3] https://www.cosmos.esa.int/web/xmm-newton/
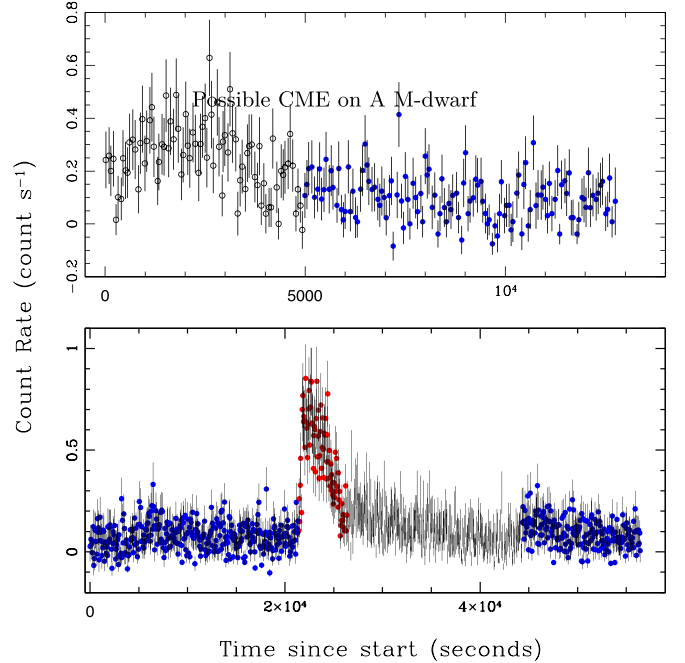
Figure 1. XMM-Newton EPIC PN X-ray light curves in 0.2–12 keV energy band. The light curves are extracted from two observation runs (Upper panel: Obs.ID = 0302150101; Lower panel: Obs.ID = 0600040101) with a binning of 60 s. The red points mark the data used for producing the flaring spectrum, and the blues ones the data for the corresponding quiescent spectrum.

3.2. Flaring and Quiescent X-Ray Spectra

The flaring and quiescent spectra are extracted from the time intervals marked by the solid red and blue points in Figure 1, respectively. A count rate enhancement at the beginning of the top light curve, which is probably due to an activity, is excluded from the quiescent spectrum extraction. Also excluded is the long tail of the flare in the lower light curve. We extract the source and background spectra by adopting the same regions used in our light curve extraction. The pile-up effect can be safely excluded after a check by using the SAS task *epatplot*. The response files needed for subsequent spectral modeling are generated by the tasks *rmfgen* and *arfgen*. With the response files, both flaring and quiescent spectra are grouped by *grppha* in HEASOFT version 6.29. The resulting spectra are depicted in the upper and lower panels in Figure 2 for the flaring and quiescent states, respectively.

3.3. Spectral Modeling

The aim of this study is to examine the signature of a flare-associated stellar CME by comparing the flaring and quiescent X-ray spectra. The spectra extracted above are then modeled here by XSPEC (v12.11, Arnaud 1996) over the 0.2–10 keV range in terms of the C-statistic (Cash 1979; Humphrey et al. 2009; Kaastra 2017).
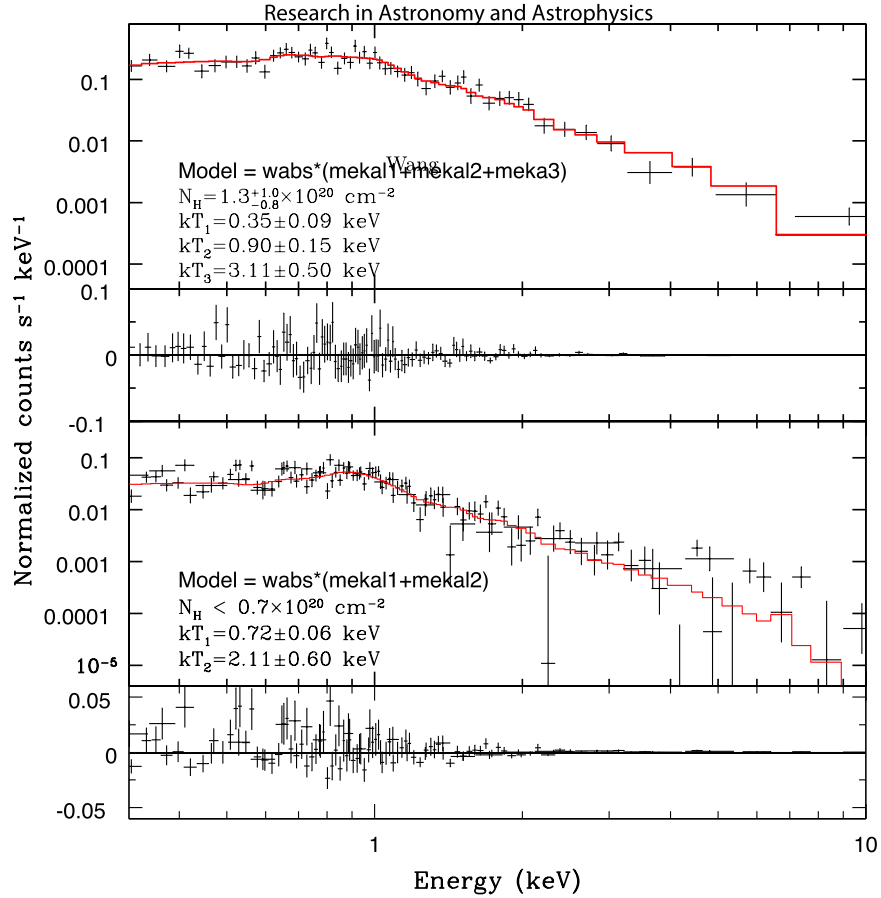
Figure 2. Upper panel: Flaring X-ray spectra of KIC 8093473 and the best-fit spectral models expressed as wabs $*$ (mekal + mekal + mekal). The subpanel underneath the spectrum shows the deviations, in units of counts s^{-1} keV^{-1}, of the observed data from the best-fit model. Lower panel: the same as the upper one, but for the quiescent state. The best-fit model is wabs $*$ (mekal + mekal).

Specifically, we reproduce the flaring spectrum by a linear combination of three optically thin thermal plasmas with different temperatures, i.e., the MEKAL model emissivities (Mewe et al. 1995). After taking into account the effect due to an interstellar (or intrinsic) absorption, the model can be expressed as wabs $*$ (mekal + mekal + mekal). Although the metal abundance determined from photometry is [Fe/H] = + 0.04 dex, the metal abundance of all the three used MEKAL components is fixed to be $0.3 Z_\odot$ in our spectral fitting because of the inadequate count rates. Most active stars, in fact, are found to have subsolar coronal metal abundance that is lower than the photospheric value (e.g., Gudel et al. 1999; Maggio et al. 2000; Gudel et al. 2001). The interstellar column density N_H is set as a free parameter in the fitting. The quiescent spectrum is fitted by a similar model except for a linear combination of only two MEKAL components.

The best fits and their parameters are displayed in Figure 2 and listed in Table 1. In the table, all of the quoted uncertainties correspond to a 1σ significance level.

Compared to the quiescent spectrum, the temperature of the hot plasma at the flaring state increases from $kT \approx 2$ keV to ≈ 3 keV. Moreover, an additional warm plasma with $kT \approx 0.3$ keV is required to reproduce the observed flaring spectrum. On the one hand, our fitting, in fact, returns a value of N_H close to zero in the quiescent spectrum. Adopting an interstellar hydrogen volume density of 0.07 cm^{-3} (Paresce 1984) yields an $N_H = 0.4 \times 10^{20}$ cm^{-2} according to the distance of the star as measured by the Gaia mission. This N_H value is consistent with the upper limit given by the modeling, which suggests an ignorable column density excess at the quiescent state. On the other hand, the N_H obtained in the flaring state is clearly higher than the interstellar value estimated above at a 1σ significance level, and marginally higher than the modeled upper limit of N_H at the quiescent state. A possible explanation for this excess is an additional obscuration due to the material expelled during the flare, which suggests a flare-associated CME occurred in the star.

Table 1
XMM-Newton EPIC PN X-Ray Spectral Fit Parameters for the Flaring and Quiescent States of KIC 8093473

Parameter (1)	Value (2)	Unit (3)	Description (4)
		Flare	
N_H	$1.3^{+1.0}_{-0.8}$	10^{20} cm^{-2}	Interstellar column density
kT_1	0.35 ± 0.09	keV	Plasma temperature
kT_2	0.90 ± 0.15	keV	Plasma temperature
kT_3	3.11 ± 0.50	keV	Plasma temperature
Cash statistic	$64.16/54 = 1.178$		
		Flare+tail	
N_H	$0.9^{+0.7}_{-0.7}$	10^{20} cm^{-2}	Interstellar column density
kT_1	0.35 ± 0.06	keV	Plasma temperature
kT_2	0.94 ± 0.16	keV	Plasma temperature
kT_3	2.47 ± 0.40	keV	Plasma temperature
Cash statistic	$114.16/118 = 0.967$		
		Quiescent	
N_H	<0.7	10^{20} cm^{-2}	Interstellar column density
kT_1	0.72 ± 0.06	keV	Plasma temperature
kT_2	2.11 ± 0.60	keV	Plasma temperature
Cash statistic	$82.39/64 = 1.287$		

4. Conclusion and Discussion

We perform a spectral analysis on the time resolved X-ray spectra of active M dwarf KIC 8093473 observed by XMM-Newton during 2005–2009. Comparison between the flare and quiescent X-ray spectra enables us to identify a marginal interstellar column density N_H excess in the flaring state. A flare-associated CME is a possible explanation for this excess (e.g., Franciosini et al. 2001; Moschou et al. 2017).

As an additional test, a spectral analysis is performed on the flaring+tail X-ray spectrum that is extracted from the time interval including both red and black points shown in the lower panel of Figure 1. The model used in the fitting is the same as that applied for the flaring spectrum. The best fit parameters are listed in Table 1 as well. One can see from the table that the inclusion of the tail results in a lower average N_H, which implies a decrease of N_H with time. In fact, a decay evolution of $N_H \propto t^{-2}$ has been revealed in the CME that occurred in the eclipsing binary Algol by Moschou et al. (2017).

We estimate the CME velocity V_{CME} in terms of the empirical relationship that is established by Salas-Matamoros & Klein (2015), see also in Moon et al. (2002), Yashiro &

Gopalswamy (2009) for solar CMEs

$$\log\left(\frac{V_{CME}}{km\ s^{-1}}\right) = (0.20 \pm 0.08)\log$$
$$\times \left(\frac{F_p}{W\ m^{-2}}\right) + (3.83 \pm 0.38), \quad (1)$$

where F_p is the peak soft X-ray flux. By assuming an observation at 1 AU from the star, the measured equivalent peak soft X-ray flux is reported to be $F_p = 1.47$ W m^{-2} by Kuznetsov & Kolotkov (2021). With this value, Equation (1) yields a $V_{CME} = (7.3 \pm 0.9) \times 10^3$ km s^{-1}, which is much larger than the velocities of 10^{2-3} km s^{-1} observed in solar CMEs (e.g., Yashiro et al. 2004).

We estimate the mass of a CME from the measured N_H in the context of the ice cream cone model (Fisher & Munro 1984) by following Moschou et al. (2017)

$$M_{CME} = \frac{V_{cone} + V_{hemi}}{b' - b} N_H \mu, \quad (2)$$

where $\mu = 1.36 m_p$ is the mass per proton for gas with solar abundance, and m_p is the rest mass of a proton. V_{cone} and V_{hemi} are the volumes of two shells, a hemispherical one and a truncated conical one (see Figure 1 and Equations (1) and (2) in Moschou et al. 2017 for the details). b' and b are the outer and inner radii of the ice cream part respectively, which can be determined from the half opening angle ω and the angular width of the shell ϕ.

The model depends on the height of the cone from the stellar center, i.e., $d = (S + R_\star)/(1 + \tan(\omega + \phi))$, where $R_\star$ is the radius of the star and S is the plasma travel distance from the stellar surface. The height increases with time as the material is ejected from the stellar surface. Zic et al. (2015) indicate that in the acceleration phase the dynamical length scale of solar CMEs have $S \sim 15 R_\odot$. By taking $S = 15 R_\star$ and assuming $\omega = 35°$ and $\phi = 10°$, the CME mass could be estimated to be $(2.1 \pm 1.9) \times 10^{20}$ g, after excluding the estimated interstellar hydrogen column density of $N_H = 0.4 \times 10^{20}$ cm^{-2}. The estimated CME mass is close to the high end of the mass range of a stellar CME compiled by Moschou et al. (2019). The estimated M_{CME} is strongly sensitive to the adopted CME length scale. A much lower mass of $M_{CME} = (7.3 \pm 6.5) \times 10^{18}$ g can be obtained if a length scale of $2R_\star$ of a typical magnetic loop is used.

Given the estimated CME mass, Figure 3 shows the location of KIC 8093473 on the bolometric energy E_{bol} versus CME mass plot. In addition to quoting the other stellar and solar events from literature directly, we obtain the value of $E_{bol} = (1.4 \pm 0.2) \times 10^{36}$ erg of KIC 8093473 from its X-ray flaring energy ($E_X = 1.35^{+0.23}_{-0.20} \times 10^{34}$ erg) reported in Kuznetsov & Kolotkov (2021) by assuming a bolometric correction of $E_X/E_{bol} = 0.01$ that is typical of the Sun (e.g., Kretzschmar 2011; Emslie et al. 2012). Similar to the other M-dwarfs
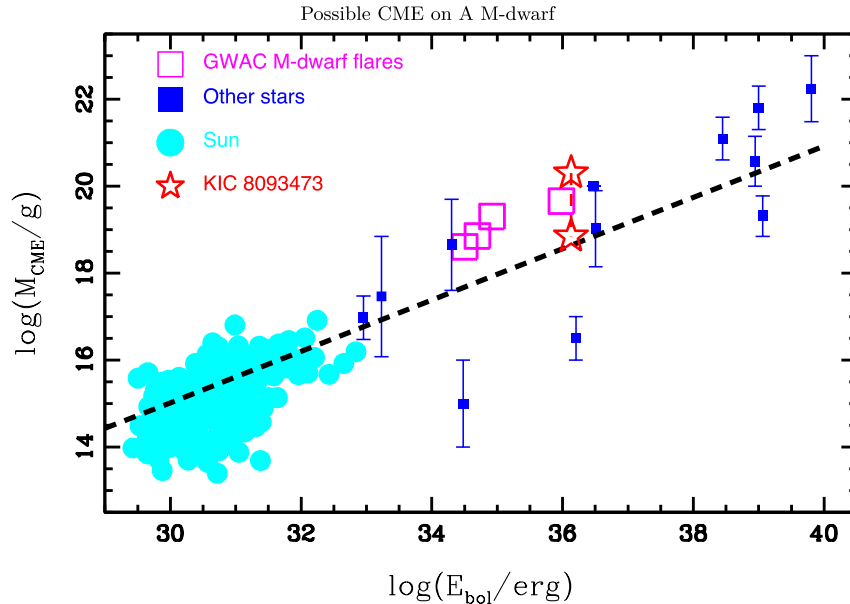
Figure 3. CME mass estimated through different ways plotted against flaring bolometric energy. KIC 8093473 is marked by the two red open stars connected by a dashed line. The two points correspond to CME masses estimated by different CME dynamical length scales (see the main text for details). The four M-dwarf flares studied in Wang et al. (2021) and Wang et al. (2022) are marked by magenta open squares. The stellar CME candidates complied in Moschou et al. (2019) and one studied in Argiroffi et al. (2019) are shown by solid blue points. The solar flare-CME events studied in Yashiro & Gopalswamy (2009) are signified by cyan circles. The best fit to these solar events obtained in Drake et al. (2013) is presented by the dashed line.

reported in Wang et al. (2021) and Wang et al. (2022), one can see from the figure that KIC 8093473 likely deviates from the best fit of the solar data by an enhanced CME mass.

We argue against a deficient CME kinetic energy in KIC 8093473 by naively estimating the kinetic energy of the CME along the line-of-sight (LoS) axis by $E_k \geqslant 1/2 M_{CME} \overline{v}^2$, where $\overline{v}$ is the mean measured LoS velocity. Combining the CME velocity estimated from Equation (1) and the CME mass yields $E_k \approx 2 \times 10^{36}$–$5 \times 10^{37}$ erg. This value is not smaller than the bolometric energy, and is comparable with the one of $E_k \approx (4.4 \pm 2.8) \times 10^{36}$ erg predicted from the solar relationship $\log E_k = (0.81 \pm 0.85) + (1.05 \pm 0.03) \log E_X$ (Drake et al. 2013). The lack of a deficient CME kinetic energy there implies a mute of the drag force done by a strong overlying magnetic field (e.g., Vrsnak et al. 2014; Zic et al. 2015).

References

Airapetian, V. S., Glocer, A., Gronoff, G., Hebrard, E., & Danchi, W. 2016, NatGe, 9, 452
Ambruster, C. W., Pettersen, B. R., & Sundland, S. R. 1989, A&A, 208, 198
Argiroffi, C., Reale, F., Drake, J. J., et al. 2019, NatAs, 3, 742
Arnaud, K. A. 1996, ASPC, 101, 17
Barnes, R., Deitrick, R., Luger, R., et al. 2016, arXiv:astro-ph/160806919
Borucki, W. J., Koch, D., Basri, G., et al. 2010, Sci, 327, 977
Cash, W. 1979, ApJ, 228, 939
Chandra, R., Chen, P. F., Fulara, A., Srivastava, A. K., & Uddin, W. 2016, ApJ, 822, 106
Cherenkov, A., Bisikalo, D., Fossati, L., & Mostl, C. 2017, ApJ, 846, 31
Drake, J. J., Cohen, O., Yashiro, S., & Gopalswamy, N. 2013, ApJ, 764, 170
Emslie, A. G., Dennis, B. R., Shih, A. Y., et al. 2012, ApJ, 759, 71
Favata, F., & Schmitt, J. H. M. M. 1999, A&A, 350, 900
Fisher, R. R., & Munro, R. H. 1984, ApJ, 280, 428
Franciosini, E., Pallavicini, R., & Tagliaferri, G. 2001, A&A, 375, 196
Giampapa, M. S., Africano, J. L., Klimke, A., et al. 1982, ApJL, 252, 39
Gudel, M., Audard, M., Briggs, K., et al. 2001, A&A, 365, L336
Gudel, M., Linsky, J. L., Brown, A., & Nagase, F. 1999, ApJ, 511, 405
Gaia Collaboration, Brown, A. G. A., Vallenari, A., et al. 2018, A&A, 616, A1
Houdebine, E. R., Foing, B. H., & Rodono, M. 1990, A&A, 238, 249
Humphrey, P. J., Liu, W. H., & Buote, D. A. 2009, ApJ, 693, 822
Jansen, F., Lumb, D., Altieri, B., et al. 2001, A&A, 365, L1
Jiang, C., Feng, X., Liu, R., et al. 2021, NatAs, 5, 1126
Kaastra, J. S. 2017, A&A, 605, 51
Kahler, S. W. 1992, ARA&A, 30, 113
Karlicky, M., & Barta, M. 2007, A&A, 464, 735
Khodachenko, M. L., Ribas, I., Lammer, H., et al. 2007, AsBio, 7, 167
Kliem, B., Karlicky, M., & Benz, A. O. 2000, A&A, 360, 715

Koller, F., Leitzinger, M., Temmer, M., et al. 2021, A&A, 646, 34

Kretzschmar, M. 2011, A&A, 530, 84

Kuznetsov, A. A., & Kolotkov, D. Y. 2021, ApJ, 912, 81

Leitzinger, M., & Odert, P. 2022, SerAJ, 205, 1

Leitzinger, M., Odert, P., Greimei, R., et al. 2014, MNRAS, 443, L898

Li, Y., Qiu, J., Longcope, D. W., Ding, M. D., & Yang, K. 2016, ApJL, 823, 13

Lu, H.-P., Tian, H., Zhang, L.-Y., et al. 2022, A&A, 663, A140

Maggio, A., Pallavicini, R., Reale, F., & Tagliaferri, G. 2000, A&A, 356, 627

Mewe, R., Kaastra, J. S., Schrijver, C. J., van den Oord, G. H. J., & Alkemade, F. J. M. 1995, A&A, 296, 477

Moon, Y.-J., Choe, G. S., Wang, H., et al. 2002, ApJ, 581, 694

Moschou, S., Drake, J. J., Cohen, O., et al. 2019, ApJ, 877, 105

Moschou, S., Drake, J. J., Cohen, O., Alvarado-Gomez, J. D., & Garraffo, C. 2017, ApJ, 850, 191

Namekata, K., Maehara, H., Honda, S., et al. 2022, NatAs, 6, 241

Osten, R. A., & Wolk, S. J. 2017, in IAUS: 328, Living Around Active Stars, ed. D. Nandy, A. Valio, & P. Petit (Maresias: Proc. IAU), 243

Paresce, F. 1984, AJ, 89, 1022

Pecaut, M. J., & Mamajek, E. E. 2013, ApJS, 208, 9

Salas-Matamoros, C., & Klein, K.-L. 2015, SoPh, 290, 1337

Shields, A. L., Ballard, S., & Johnson, J. A. 2016, PhR, 663, 1

Struder, L., Briel, U., Dennerl, K., et al. 2001, A&A, 365, L18

Tian, F., Kasting, J. F., & Zahnle, K. 2011, E&PSL, 308, 417

Tsuneta, S. 1996, ApJ, 456, 840

Van Cleve, J. E. , Howell, S. B., Smith, J. C., et al. 2016, PASP, 128, 075002

Veronig, A. M., Odert, P., Leitzinger, M., et al. 2021, NatAs, 5, 697

Vrsnak, B., Temmer, M., Zic, T., et al. 2014, ApJS, 213, 21

Wang, J., Li, H. L., Xin, L. P., et al. 2022, ApJ, 934, 98

Wang, J., Xin, L. P., Li, H. L., et al. 2021, ApJ, 916, 92

Wu, Y., Chen, H., Tian, H., et al. 2022, ApJ, 928, 180

Yang, H. Q., & Liu, J. F. 2019, ApJS, 241, 29

Yashiro, S., & Gopalswamy, N. 2009, IAUS, 257, 233

Yashiro, S., Gopalswamy, N., Michalek, G., et al. 2004, JGRA, 109, 7105

Zic, T., Vrsnak, B., & Temmer, M. 2015, ApJS, 218, 32